SILAR DEPOSITED HGS NANOPARTICLES TOWARDS STABILIZED ENERGY EFFICIENT SUPERCAPACITOR APPLICATION

SHILPA A. PANDE

Dept of Applied Physics, Laxminarayan Institute of Technology, R T M Nagpur University,
Nagpur 440033, Maharashtra, India
E-mail: sap7001@gmail.com

Abstract - Efforts have been put forth to grow HgS nanoparticles through simple and low-cost successive ionic layer adsorption and reaction (SILAR) method at room temperature towards supercapacitive electrode application. Maximum specific capacitance of 446 F/g was obtained in cyclic voltammetry measurement at 2 mV/s scan rate in 1 M KCl electrolyte. After initial drop of capacitance up to 500 cycles, reduction was relatively slow up to 2000 cycles during stability analysis. Most importantly, the revealed specific energy of 15.45 Wh/kg of electrode has promised as decent electrode in energy storage field for future scope.

Keywords - Mercury Sulfide, Thin Film, Nanoparticles, Supercapacitor

Supercapacitors are emerging as devices of prime importance owing to their superior characteristics unmatched by any other charge storage device which includes: high power densities at relatively high energy densities and long cycle life. Supercapacitors are now widely used in hybrid electric vehicles along with the improvement in transportation field[1]. Metal sulphides are also known to be electrochemically active materials for supercapacitor applications. But as on date very few metal sulfides, such as MoS_2, CuS, ZnS, etc. have been employed to fabricate supercapacitor electrodes[2].

Mercury sulphide (HgS) shows a variety of applications in many fields such as electrostatic imaging, ultrasonic transducing, image sensors, and photoelectric conversion devices [3]. Further HgS contains narrow band gap, therefore it is a promising material for applications in catalysts and infrared detectors [4]. Many researchers have taken keen investigative interest in physical properties of nanometer size (20–80 nm) semiconductor clusters due to their novelty; their properties are different and superior to those of conventional coarse-grained polycrystalline materials and also amorphous alloys of the same composition in addition to increased strength, hardness, enhanced diffusivity, improved quality, roughness, reduced elastic modulus, higher thermal expansion coefficient, lower thermal conductivity and superior soft magnetic properties [5, 6].

Recently, many researchers have synthesized HgS thin films by various deposition methods of preparing chalcogenides[3, 4, 7,8]. However, the study of HgS thin film towards supercapacitor application has not been undertaken by any researchers. Hence, attempt has been focussed to synthesize HgS nanoparticles in thin film form towards supercapacitor application. Current investigation includes (i) Demonstration of simple and scalable chemical route, namely SILAR to achieve highly porous and stable HgS thin film on conducting stainless steel (SS), (ii) Nanoporous surface architecture affords advanced electro-active porous cavities for electrolyte ions, the diffusion and relaxation time constants of the film have been evaluated to get in depth understanding of the superior performance, and (iii) Higher values of specific capacitance, specific energy/power with modest cyclic stability of electrode.

Synthesis of HgS was carried out as per previous report [9]. In brief, 0.1 M $(CH_3COO)_2Hg$complexed with a few drops of Triethanolamine (TEA) and ammonia (30%) with resultant pH~8 was used as cationic solution. Whereas, 0.1 M of Na_2S solution (pH ~ 12) was used as anionic precursor. The cationic precursor solution releases Hg^{2+} ions from $[Hg(CH_3COO)]^{2+}$ as

$$[Hg(CH_3COO)_2]^{2+} \longrightarrow Hg^{2+} + CH_3COO^- \quad (1)$$

Well cleaned stainless steel (SS) substrate was immersed into cationic precursor for 10 s to adsorb Hg^{2+} ions due to Van-der-Waals, chemical or cohesive forces [10].In the anionic precursor solution, sodium sulphide hydrolyzes to give S^{2-}ions. When steel substrate was immersed into the sodium sulfide (Na_2S) solution, sulfide ions (S^{2-}) are reacted with adsorbed mercury ions (Hg^{2+}) to form thin film of HgS

$$Hg^{2+} + S^{2-} \longrightarrow \underset{\downarrow}{HgS} \quad (2)$$

Finally, the unreacted ions ($S^{2-}$and Hg^{2+}) were separated out by rinsing the substrate in double distilled water. After few number of such SILAR cycles, uniform HgS thin film was formed with optimum thickness and used for further characterizations.

XRD pattern of HgS thin film is shown in Fig. 1a where the presence of prominent peaks at 2θ = 26.28, 30.42, and 64.42° confirm the existence of (111), (200) and (400) planes, respectively for the cubic structure with referenced to JCPDS Card No. 65-2888. The other peaks marked by 'Δ' assigned due to reflections from SS substrate. The average crystallite size was calculated as 22 nm using the Scherrer formula [13].

Chemical state was examined through XPS which exhibited the presence of S2s, S2p and Hg4f core level signals as shown in Fig. 1b. High-resolution XPS (HRXPS) spectra of $Hg4f_{(7/2, 5/2)}$, $S2p_{(3/2, 1/2)}$ and $S2s_{(1/2)}$ core levels of HgS are shown in Fig. 1c,d. Furthermore, the Hg 4f spectrum has a doublet feature due to spin orbit splitting resulting in $4f_{7/2}$ and $4f_{5/2}$ peaks at 99.90 and 103.88 eV, respectively (Fig. 1c). No peaks of impurities such as those of oxide or metallic mercury were found in the spectrum, indicating the high purity of the formed HgS. The presence of S2s can be confirmed by distinct peaks at 225.5 eV. This XPS results are well matched with previously reported articles [14, 15].

FESEM images of the HgSnanocrystals shows nanoparticles with an average grain diameter of 20 nm (Fig. 2a, b). Morphology reveals cauliflower like surface architecture with microporous structure leading to high surface area which facilitates more active sites for electrolyte ions. The compositions of the chemically prepared HgS samples on stainless steel substrate were analysed by energy dispersive X-ray analysis (EDAX) (Supplementary information S3).

HRTEM images in Fig. 2c, d demonstrate the spherical nanocrystallites and high-dispersity of the HgS nanoparticles. The fringes with a lattice spacings of 0.33, 0.29, and 0.14 nm are clearly observed in Fig. 2d which corresponds to (111), (200), and (400) planes respectively. The Bragg spots contained ring-like SAED diffraction pattern confirms the crystalline (200) and (400) planes of HgS nanoparticles (Fig. 2d, inset).The diffraction planes analysed from the SAED pattern are in excellent agreement with that obtained from XRD measurements.

In order to find suitable electrolyte for superior electrochemical behavior, the CV curves of HgS thin film were recorded in 0.5 M solution of Na_2SO_4, Na_2SO_3, KCl, K_2SO_4, NaOH, KOH, LiCl and $LiClO_4$ electrolytes at scan rate of 100 mV/s (Fig. 3a). The CV curve of HgS thin film exhibited a rectangular-shaped profile in 0.5 M LiCl whereas portray pseudocapacitance aligned non-rectangular shape for 0.5 M aqueous solution of Na_2SO_4, Na_2SO_3, KCl and NaOH, respectively. The highest specific capacitance of has been calculated in aqueous KCl solution with faradic charge-discharge, indicating its suitability for HgS thin film.

For optimum KCl electrolyte concentration, the electrolyteconcentration was varied from 0.1 to 1 M (Fig. 3b) by keeping the scan rate and potential window constant (100 mV/s and 0-0.6 V). The current under the curve increases with increase concentration of KCl from 0.5 to 1.0 M. However, with the further increase in concentration, the ionic activity may be reduced due to less water hydration resulting in decrease ion mobility[16].Hence, the electrochemical properties of the HgS electrode were investigated in 1 M KCl.

Fig. 3c depicts the CV curves in 1 M KCl where a pair of redox peaks has been visualised indicating oxidation (0.32 V) and reduction (0.11 V) electrochemical behaviour (Faradaic redox responses) at scan rate from 2 to 100 mV/s which can be ascribed to the following reaction kinetics

$$HgS + xK^+ + xe^- \rightleftharpoons K_xHgS \qquad (3)$$

It can be observed that the peak current densities increase with increasing in the scan rate; suggesting perfect capacitive behavior. The maximum specific capacitance (based on active mass as 0.31 mg/cm^2) obtained as 446 F/g at the scan rate of 2mV/s. Due to the limitation of time constraints, the capacitance value decreases at higher scan rates; resulting in 210 F/g specific capacitance at of 100 mV/s scan rate [17].

Fig. 3d shows the Galvanostatic charge discharge (GCD) curves which exhibit almost asymmetric shape, indicating the pseudo-capacitive behavior of the electrodes. The initial potential drop (IR drop) in discharge curve was the result of internal resistance loss. The durations of charge and discharge are nearly equal, indicating high reversibility. The specific capacitance reaches 309 F/g at the current density of 1.24 A/g. Using the discharge curves, specific energy and specific power were calculated through the Ragone plot (Fig. 4a). Impressively, the plot demonstrates the high specific energy of 15.45 Wh/kg at specific power of 0.98 kW/kg for the specific current of 1.24 A/g which is quite encouraging for the framework of developing HgS as active electrode material for supercapacitor application.

Towards the practical applicability, the cycling stability of HgS electrode was undertaken for 2000 cycles at 100 mV/s scan rate and depicts as variation of capacitance retention with cycle number Fig. 4b. Degradation of active electrode material during electrochemical activity to the electrolyte is a serious issue for pseudo-capacitive material. It can be seen that for the capacitance suddenly decreases to70% up

to the first 500 cycles and then remains almost 55 % upto 2000 cycles indicating modest electrochemical stability. Furthermore, the unchanged redox influenced shape of CV curves even after 2000 cycles strongly demonstrates the excellent rate capability and sustainability of the active electrode [18].

The electrochemical impedance spectrum (EIS) for HgS electrode with corresponding equivalent circuit is shown in Fig. 4c. The X-axis intercept and small arc in Nyquist curve at high frequency the curve indicates solution resistance (R_S) and charge transfer resistance (R_{CT}), respectively [17]. Here the HgS electrode shows a very low value of R_S and R_{CT} as 1.3 Ω/cm^2 and 5.9 Ω/cm^2 respectively which facilitate faster electron transport of during charge-discharge. The parallel connection of double layer capacitance (C_{DL}) and R_{CT} represents small arc in high frequency region of Nyquist curve whereas the inclination of curve to some angle with real axis signifies combine posture of mass capacitance (C_L) and leakage resistance (R_L) [19]. The Warburg component (W) defines the disseminated resistance of HgS electrode.

The phase angle as a function of frequency is mentioned as Bode plot which is important tool to elucidate the quality of active electrode material. An idyllic capacitive component indicates exact -90° phase angle [20]. From the Fig. 4d, it is appreciated that the phase angle is close to -77° in frequency frame of impedance scrutiny; suggesting perfect capacitive behavior of HgS electrode.

In summary, HgS thin film has been synthesized by simple, low-cost SILAR route and employed as a supercapacitive electrode. Room temp synthesized HgS thin film confirms the formation of nanocrystalline cubic phase with particle size around 20 nm, favourable for superior electrochemical characteristics towards energy storage application and exhibited an enhanced specific capacitance of 446 F/g and higher energy density of about 15.45 Wh/kg with modest cyclic life-span. These encouraging results suggest that the HgS electrode can serve as promising electrode material for future energy storage applications.

ACKNOWLEDGEMENTS

The authors gratefully acknowledge the support of STIC, Cochin, and VNIT, Nagpur for providing the facilities to carry out this work.

REFERENCES

[1] B. Dong, B.-L. He, C.-L. Xu, H.-L. Li, Materials Science and Engineering: B 143(1–3) (2007) 7-13.
[2] X. Rui, H. Tan, Q. Yan, Nanoscale 6(17) (2014) 9889-9924.
[3] S.S. Kale, C.D. Lokhande, Mater. Chem. Phys. 59(3) (1999) 242-246.
[4] F.S. Sangsefidi, M. Esmaeili-Zare, M. Salavati-Niasari, Journal of Industrial and Engineering Chemistry 28 (2015) 197-201.
[5] C.D. Lokhande, B.R. Sankapal, H.M. Pathan, M. Muller, M. Giersig, H. Tributsch, Appl. Surf. Sci. 181(3–4) (2001) 277-282.
[6] C. Suryanarayana, Bull. Mater. Sci. 17(4) (1994) 307-346.
[7] R.S. Patil, T.P. Gujar, C.D. Lokhande, R.S. Mane, S.-H. Han, Solar Energy 81(5) (2007) 648-652.
[8] K.J. Siemsen, H.D. Riccius, physica status solidi (b) 37(1) (1970) 445-451.
[9] R.S. Patil, C.D. Lokhande, R.S. Mane, H.M. Pathan, O.-S. Joo, S.-H. Han, Materials Science and Engineering: B 129(1–3) (2006) 59-63.
[10] s. karade, P. Dwivedi, S. Majumder, B. Pandit, B.R. Sankapal, Sustainable Energy & Fuels (2017). https://doi.org/10.1039/C7SE00165G.
[11] B.R. Sankapal, H.B. Gajare, S.S. Karade, D.P. Dubal, RSC Adv. 5(60) (2015) 48426-48432.
[12] S. Roldan, D. Barreda, M. Granda, R. Menendez, R. Santamaria, C. Blanco, PCCP 17(2) (2015) 1084-1092.
[13] R.S. Mane, B.R. Sankapal, C.D. Lokhande, Thin Solid Films 359(2) (2000) 136-140.
[14] R. Selvaraj, K. Qi, S.M.Z. Al-Kindy, M. Sillanpaa, Y. Kim, C.-W. Tai, RSC Adv. 4(30) (2014) 15371-15376.
[15] G. Marimuthu, M. Arivanandhan, C. Vedhi, Synthesis and Reactivity in Inorganic, Metal-Organic, and Nano-Metal Chemistry 45(2) (2015) 217-224.
[16] K.-C. Tsay, L. Zhang, J. Zhang, Electrochim. Acta 60 (2012) 428-436.
[17] B. Pandit, D.P. Dubal, B.R. Sankapal, Electrochim. Acta (2017). https://doi.org/10.1016/j.electacta.2017.05.010.
[18] T. Wang, S. Chen, H. Pang, H. Xue, Y. Yu, Advanced Science 4(2) (2017) 1600289-n/a.
[19] B. Pandit, D.P. Dubal, P. Gómez-Romero, B.B. Kale, B.R. Sankapal, Sci. Rep. 7 (2017) 43430.
[20] H. Peng, G. Ma, K. Sun, J. Mu, M. Luo, Z. Lei, Electrochim. Acta 147 (2014) 54-61.

Figure Captions

Figure 1 (a) XRD patterns of bare stainless steel (ss) and HgS/SS thin film, (b) survey spectrum of HgS, (c, d) core level XPS spectrum of HgS for Hg4f and S2p Figure 2 FESEM images of HgS/SS thin film at (a) 2 μm and (b) 100 nm, HRTEM image of HgS sample at (c) 20 nm and (d) 2 nm, inset shows SAED patterns of HgS.

Figure 3 (a) CV Curves of HgS at different electrolytes, inset shows variation of specific capacitance with different electrolytes, (b) effect of KCl electrolyte concentrations on CV curves at 100 mV /s scan rate, inset shows variation of specific capacitance with different KCl concentrations, (c) CV curves of HgS electrode at different scan rates in 1

M KCl, inset shows specific capacitance as a function of scan rate, (e) Galvanostatic charge–discharge curves of the HgS electrode at different current densities, inset shows specific capacitance as a function of current density Figure 4 (a) Ragone Plot, (b) Cycling stability for 2000 cycles, inset shows CV curves for different cycle numbers at a scan rate of 100 mV/s, (c) Nyquist plot with equivalent circuit, inset shows an enlarged view of the high-frequency region, (d) Bode plot of phase angles

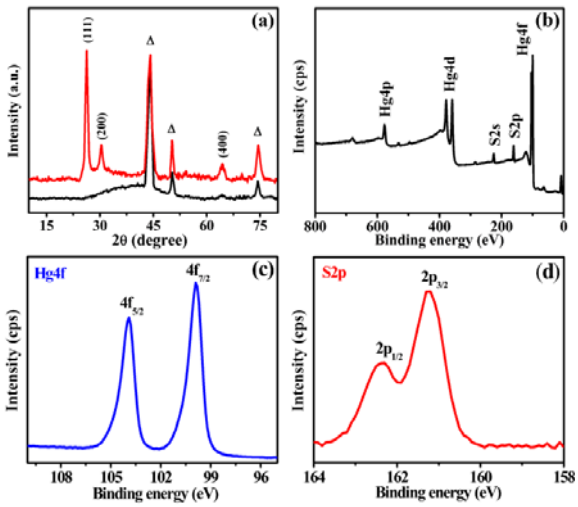


Figure 1

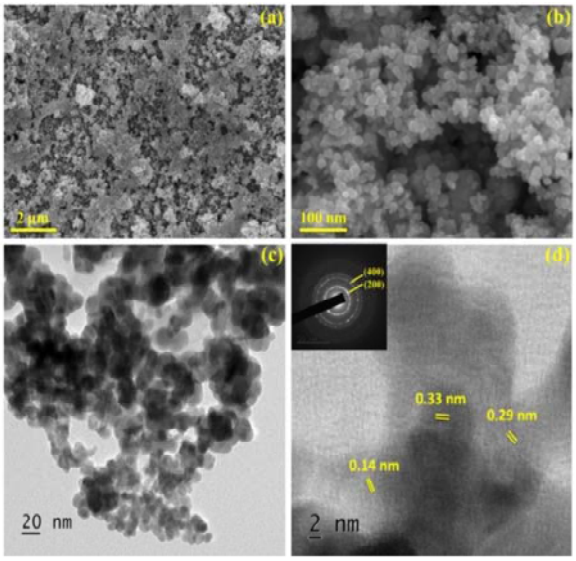


Figure 2

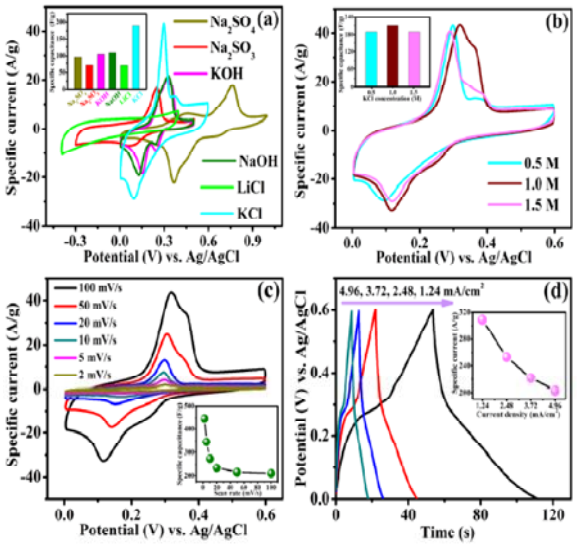


Figure 3

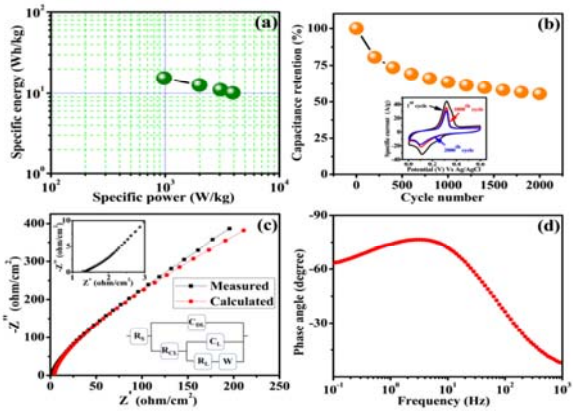


Figure 4

★★★